APPLIED GEOPHYSICS, Vol.13, No.2 (June 2016), P. 279-287, 5 Figures.
DOI:10.1007/s11770-016-0560-2

Forward modeling of marine DC resistivity method for a layered anisotropic earth*

Yin Chang-Chun[1], Zhang Ping♦[1], and Cai Jing[1]

Abstract: Since the ocean bottom is a sedimentary environment wherein stratification is well developed, the use of an anisotropic model is best for studying its geology. Beginning with Maxwell's equations for an anisotropic model, we introduce scalar potentials based on the divergence-free characteristic of the electric and magnetic (EM) fields. We then continue the EM fields down into the deep earth and upward into the seawater and couple them at the ocean bottom to the transmitting source. By studying both the DC apparent resistivity curves and their polar plots, we can resolve the anisotropy of the ocean bottom. Forward modeling of a high-resistivity thin layer in an anisotropic half-space demonstrates that the marine DC resistivity method in shallow water is very sensitive to the resistive reservoir but is not influenced by airwaves. As such, it is very suitable for oil and gas exploration in shallow-water areas but, to date, most modeling algorithms for studying marine DC resistivity are based on isotropic models. In this paper, we investigate one-dimensional anisotropic forward modeling for marine DC resistivity method, prove the algorithm to have high accuracy, and thus provide a theoretical basis for 2D and 3D forward modeling.
Keywords: Electrical anisotropy, Marine DC resistivity method, Forward modeling, Field continuation algorithm

Introduction

The ocean bottom is rich in mineral resources, oil, and gas which can be exploited as effective extensions of land-based resources. In recent years, marine geophysical exploration technology has rapidly developed for use in seabed exploration. In one such technology—the marine DC resistivity method—direct current is applied to the sea floor, the electric field is then measured, and the apparent resistivity calculated. This method has been widely used in mineral, seafloor permafrost, and oil and gas explorations.

In the mid-1950s, the former Soviet Union carried out dipole electric soundings in the Caspian Sea, which demonstrated the feasibility of the marine DC electrical method (Fedynskiy, 1960). Lile et al. (1994) used the DC resistivity method to detect Norwegian subsea bedrock faults, and the authors successfully delineated fracture zones and mitigated risk in submarine tunnel construction. Von Herzen et al. (1996) used the DC resistivity method in submarine exploration to survey the distribution of sulfide deposits in formations located at water depths of over 3600 m. Inoue (2005) developed

Manuscript received by the Editor March 13, 2016; revised manuscript received June 12, 2016.
*This paper is financially supported by the National Hi-tech Research and Development Program of China (863 Program) (No. 2012AA09A20103).
1. College of Geo-Exploration Science and Technology, Jilin University, Changchun 130026, China.
♦Correspondence author: Zhang Ping (Email:zhangping_1@126.com)
© 2016 The Editorial Department of **APPLIED GEOPHYSICS**. All rights reserved.

and improved a new marine electrical sounding system, which was applied in a shallow-water DC resistivity survey. Kwon et al. (2005) used a floating electrode to explore and delineate a shallow-water fault zone. Allen and Merrick (2007) studied the 1D inversion of a shallow-water towed DC resistivity system, and this method was shown to effectively deal with data having a low signal-to-noise ratio. Goto et al. (2008) developed a new deep-water marine DC resistivity system and used it to prospect for carbohydrates near the Sea of Japan. Tarits et al. (2012) designed a survey system that can map the resistivity distribution of the sea bottom and demonstrated good performance in the observation of the main lithology and free gas in shallow seas. Goto et al. (2013) used a remotely operated vehicle (ROV) to analyze the distribution of massive sulfide deposits in Okinawa waters off southwestern Japan. Xu and Dunbar (2015) digitalized irregular continuous resistivity profiling (CRP) data into a regular grid, thereby achieving a 3D shallow-sea DC resistivity inversion.

In the past, marine DC and electromagnetic (EM) theory has relied on an isotropic earth model. However, marine sedimentary strata demonstrate varying degrees of anisotropy. Matias and Habberjamz (1986) analyzed the influence of electrical anisotropy on DC resistivity data. Li and Pedersen (1991) used vector and scalar potentials to calculate the EM responses for an azimuthally anisotropic earth. Weidelt (1999) used the finite difference technique to realize an EM response for an anisotropic model. Yin and Weidelt (1999) developed an algorithm for modeling the DC resistivity of an anisotropic medium and studied the directional variation of the apparent resistivity in anisotropic media. In 2006, Yin investigated the characteristics of marine magnetotelluric (MMT) apparent resistivity and phase for an arbitrarily anisotropic ocean bottom. Kong et al. (2008) developed a marine controlled-source anisotropic modeling algorithm using finite element analysis, which can effectively reduce the near-field error caused by the singularity of the transmitting dipole. Um et al. (2010) proposed a 3D finite element time domain (FETD) method for simulating the transient EM field in an anisotropic model. Compared to the original FDTD method, both the efficiency and accuracy were improved. Newman et al. (2010) used the non-linear conjugate gradient method to invert marine controlled-source EM (MCSEM) data from a transversely isotropic medium. Wang et al. (2011) used an unstructured finite-element method to calculate 3D DC resistivity in anisotropic models and analyzed the characteristics of the apparent resistivity. A 3D-edge finite-element method was proposed by Cai et al. (2014) for modeling the anisotropic EM responses of the marine controlled-sourced electromagnetic (MCSEM) method. Yin et al. (2014) used a 3D staggered-grid finite-difference method to study 3D MCSEM forward modeling in an arbitrarily anisotropic model. Zhou et al. (2015) proposed a method that used difference fields to reduce the source singularity of anisotropic formations. However, to date, there have been no forward modeling results published regarding the use of the marine DC resistivity method in an arbitrarily anisotropic model. In this paper, we apply the continuation algorithm developed by Yin and Weidelt (1999) to realize forward modeling of the marine DC resistivity method in a 1D anisotropic model. First, we introduce two scalar potentials based on the divergence-free properties of the electric and magnetic fields. Then, we use the continuity conditions of the electric and magnetic fields at the layer interfaces to achieve downward and upward continuation of the EM field. We couple the EM field to the transmitting dipole at the ocean bottom to solve the EM field. Using a dipole-dipole array as an example, we then verify the effectiveness of our algorithm. We also examine the influence of electrical anisotropy on marine DC resistivity and develop a technique to identify the electrical anisotropy of the sea floor from the apparent resistivity distributions. Finally, we identify oil and gas reservoirs from the anisotropic seabed background by forward modeling in different oil and gas reservoir models in an anisotropic environment.

Basic equation

In the DC resistivity method, the Maxwell equations are simplified as follows:

$$\begin{aligned} \nabla \times \mathbf{E} &= 0, \qquad \nabla \cdot \mathbf{J} = 0, \\ \nabla \times \mathbf{H} &= J, \qquad \nabla \cdot \mathbf{B} = 0, \end{aligned} \tag{1}$$

where $\mathbf{E}$ is the electric field, $\mathbf{H}$ is the magnetic field, $\mathbf{J}$ is the current density, and $\mathbf{B}$ is the magnetic induction. $\mathbf{J} = \sigma\mathbf{E} + \mathbf{J}_e, \sigma = \rho^{-1}$, and $\mathbf{J}_e$ is the source current density. For an arbitrarily anisotropic medium, the resistivity tensor can be expressed as follows (Yin, 2000):

$$\rho = \begin{bmatrix} \rho_{xx} & \rho_{xy} & \rho_{xz} \\ \rho_{xy} & \rho_{yy} & \rho_{yz} \\ \rho_{xz} & \rho_{yz} & \rho_{zz} \end{bmatrix}. \tag{2}$$

The symmetric positive-definite resistivity tensor can be obtained by the three Euler rotations of the principal electrical resistivity tensor (Yin, 2000). Due to the divergence-free feature of the electric and magnetic fields in equation (1), we introduce a toroidal and a poloidal scalar potential. Then, the EM field is expressed as follows (Yin and Maurer, 2001):

$$\mathbf{H} = \nabla \times (\hat{\mathbf{z}} T_H) + \nabla \times \nabla \times (\hat{\mathbf{z}} P_H),$$
$$\mathbf{J} = \nabla \times (\hat{\mathbf{z}} T_J) + \nabla \times \nabla \times (\hat{\mathbf{z}} P_J). \quad (3)$$

In the above equations, T_J, T_H are toroidal scalars, while P_J, P_H are poloidal scalars. $\hat{\mathbf{z}}$ is a positive-downward unit vector with the sea bottom as the origin of the Cartesian coordinate system. In the wave number domain, we have:

$$F(x,y) = \frac{1}{4\pi^2} \int\int_{-\infty}^{+\infty} \tilde{F}(u,v) e^{i(ux+vy)} du dv, \quad (4)$$

where $\mathbf{k} = u\hat{\mathbf{x}} + v\hat{\mathbf{y}} = k(\hat{\mathbf{x}}\cos\beta + \hat{\mathbf{y}}\sin\beta)$, and $k, \hat{\mathbf{x}}, \hat{\mathbf{y}}$ are, respectively, the wave number and the unit vectors in the x-axis and y-axis directions. With equation (4), the EM field in equation (3) is expressed as follows:

$$\tilde{\mathbf{J}} = \begin{pmatrix} iv\tilde{T}_J + iu\tilde{P}_J' \\ -iu\tilde{T}_J + iv\tilde{P}_J' \\ k^2\tilde{P}_J \end{pmatrix}, \quad \tilde{\mathbf{H}} = \begin{pmatrix} iv\tilde{T}_H + iu\tilde{P}_H' \\ -iu\tilde{T}_H + iv\tilde{P}_H' \\ k^2\tilde{P}_H \end{pmatrix}, \quad (5)$$

where the prime denotes the derivative with respect to the z-coordinate. Using equation (1), we have:

$$\tilde{T}_H = \tilde{P}_J, \quad \tilde{T}_J = k^2\tilde{P}_H - \tilde{P}_H'', \quad (6)$$

and equation (5) is then changed to:

$$\tilde{\mathbf{J}} = \begin{pmatrix} i[v(k^2\tilde{P}_H - \tilde{P}_H'') + u\tilde{P}_J'] \\ i[-u(k^2\tilde{P}_H - \tilde{P}_H'') + v\tilde{P}_J'] \\ k^2\tilde{P}_J \end{pmatrix}, \tilde{\mathbf{H}} = \begin{pmatrix} i[v\tilde{P}_J + u\tilde{P}_H'] \\ i[-u\tilde{P}_J + vP_H'] \\ k^2\tilde{P}_H \end{pmatrix}. \quad (7)$$

For a layered earth model, the resistivity changes only in the vertical direction. Thus, we have:

$$\hat{\mathbf{z}} \cdot \nabla \times \mathbf{E} = \hat{\mathbf{z}} \cdot \nabla \times (\rho\mathbf{J}) = 0,$$
$$\hat{\mathbf{z}} \cdot \nabla \times \nabla \times \mathbf{E} = \hat{\mathbf{z}} \cdot \nabla \times \nabla \times (\rho\mathbf{J}) = 0. \quad (8)$$

Combining equation (6) and (8), we can obtain:

$$a\tilde{P}_H'' - k^2 a\tilde{P}_H - b\tilde{P}_J' + ic\tilde{P}_J = 0,$$
$$d\tilde{P}_J'' + 2e\tilde{P}_J' + (c^2 - af)\tilde{P}_J = 0, \quad (9)$$

where

$$a = \rho_{xx}\sin^2\beta - 2\rho_{xy}\sin\beta\cos\beta + \rho_{yy}\cos^2\beta,$$
$$b = \rho_{xy}(\sin^2\beta - \cos^2\beta) + (\rho_{xx} - \rho_{yy})\sin\beta\cos\beta,$$
$$c = k(\rho_{xz}\sin\beta - \rho_{yz}\cos\beta),$$
$$d = \rho_{xx}\rho_{yy} - \rho_{xy}^2,$$
$$e = ik[(\rho_{xz}\rho_{xy} - \rho_{yz}\rho_{xx})\sin\beta + (\rho_{yz}\rho_{xy} - \rho_{xz}\rho_{yy})\cos\beta],$$
$$f = \rho_{zz}k^2. \quad (10)$$

Assuming $\tilde{P}_H = A_H e^{-\alpha z}$, $\tilde{P}_J = A_J e^{-\alpha z}$ in equation (9), with A_H, A_J denoting the amplitudes, we obtain:

$$\begin{pmatrix} \alpha^2 a - k^2 a & \alpha b + ic \\ 0 & \alpha^2 d - 2\alpha e + c^2 - af \end{pmatrix} \begin{pmatrix} A_H \\ A_J \end{pmatrix} = \begin{pmatrix} 0 \\ 0 \end{pmatrix}. \quad (11)$$

Since the amplitudes of the EM fields in equation (11) are not vanishing, meaning that there are no trivial solutions for the EM fields, the determinant of the coefficient matrix must be zero, so we obtain the solutions for α (Bronstein and Semendjajew, 1979). Note that α has four solutions, with each positive and negative pair denoting upward and downward traveling waves. From equation (11), we can define the amplitude ratio: $\gamma_m = A_{J_m}/A_{H_m} = (-\alpha_m^2 a + k^2 a)/(\alpha_m b + ic)$. The EM scalar potentials in layer l of the seafloor medium ($z_l \le z \le z_{l+1}$) can be expressed as follows:

$$\tilde{P}_{Hl} = \sum_{m=1}^{4} A_{ml}^- e^{-\alpha_{ml}(z-z_l)}, \quad \tilde{P}_{Jl} = \sum_{m=1}^{4} \gamma_{ml} A_{ml}^- e^{-\alpha_{ml}(z-z_l)}. \quad (12)$$

The boundary conditions for the EM fields at the layer interfaces are as follows:

$$\left[\tilde{P}_H\right] = 0, \left[\tilde{P}_H'\right] = 0, \left[\tilde{P}_J\right] = 0, \left[(d\tilde{P}_J' + e\tilde{P}_J)/a\right] = 0, \quad (13)$$

where [ ] denotes a change of the scalar potential at the interface. From equations (12) and (13), we can use the algorithm developed by Yin and Weidelt (1999) to achieve the downward continuation of the electromagnetic fields. Similarly, we can solve for the EM field in seawater. Assuming the seawater depth is h_0, we have:

$$\tilde{P}_H = A_H e^{kz}, \qquad -h_0 \le z \le 0,$$
$$\tilde{P}_J = A_J (e^{kz} - e^{-k(2h_0+z)}), \quad -h_0 \le z \le 0. \tag{14}$$

Due to the presence of a transmitting dipole at the sea bottom, the scalar potentials are discontinuous. According to Yin and Maurer (2001), we have:

$$\left[\tilde{P}_J\right]_-^+ = \tilde{P}_J(0^+) - \tilde{P}_J(0^-) = D_J,$$
$$\left[\tilde{P}_H'\right]_-^+ = \tilde{P}_H'(0^+) - \tilde{P}_H'(0^-) = D_H, \tag{15}$$

where

$$D_J = \frac{I}{k^2}\left\{e^{-i\mathbf{k}\cdot\mathbf{r}_A} - e^{-i\mathbf{k}\cdot\mathbf{r}_B}\right\}, \tag{16}$$

$$D_H = \begin{cases} -\dfrac{I}{k^2}\dfrac{(\mathbf{k}\times\hat{\mathbf{z}})\cdot\hat{\mathbf{d}}}{\mathbf{k}\cdot\hat{\mathbf{d}}}\left\{e^{-i\mathbf{k}\cdot\mathbf{r}_A} - e^{-i\mathbf{k}\cdot\mathbf{r}_B}\right\}, & \mathbf{k}\cdot\hat{\mathbf{d}} \neq 0, \\ \dfrac{I}{k^2} i(\mathbf{k}\times\hat{\mathbf{z}})\cdot\hat{\mathbf{d}}\left|\mathbf{r}_A - \mathbf{r}_B\right| e^{-i\mathbf{k}\cdot(\mathbf{r}_A+\mathbf{r}_B)/2}, & \mathbf{k}\cdot\hat{\mathbf{d}} = 0. \end{cases} \tag{17}$$

In the above equations, I denotes the transmitting current, while $\mathbf{r}_A = (x_A, y_A, 0), \mathbf{r}_B = (x_B, y_B, 0)$ denotes the position of the two ends of the transmitting dipole. By inserting equations (12) and (14) into (15), we obtain $\tilde{P}_J$ and $\tilde{P}_H$ in each layer of the medium. Then, from equation (7) we can obtain the current density. Via Ohm's law, we can further obtain the electric field in the earth under the ocean, i.e.,

$$\begin{pmatrix} \tilde{E}_{xl} \\ \tilde{E}_{yl} \\ \tilde{E}_{zl} \end{pmatrix} = \begin{pmatrix} \rho_{xxl} & \rho_{xyl} & \rho_{xzl} \\ \rho_{xyl} & \rho_{yyl} & \rho_{yzl} \\ \rho_{xzl} & \rho_{yzl} & \rho_{zzl} \end{pmatrix} \begin{pmatrix} \tilde{J}_{xl} \\ \tilde{J}_{yl} \\ \tilde{J}_{zl} \end{pmatrix}. \tag{18}$$

Using the above mathematical formulations, we can model the marine DC resistivity for an arbitrarily anisotropic earth under the ocean. This provides the means for modeling a towed marine DC resistivity system. Weng and Zhu (2010) compared different arrays of the marine DC resistivity method and found that different arrays have different degrees of resolvability with respect to anomalous targets under the seafloor, with the dipole–dipole array being the best. Thus, in the following, we mainly discuss the dipole–dipole array. We put the transmitting dipole along the *x*-axis, *A* and *B* denote current electrodes (symmetric about the origin), and *M* and *N* denote potential electrodes. The distance between the transmitting and receiving dipoles is $r_0 = na$. The apparent resistivity is as follows:

$$\rho_a = \pi n(n+1)(n+2)a\frac{\Delta V}{I}, \tag{19}$$

where $AB = MN = a$.

Numerical results

Accuracy check

To verify the accuracy of the algorithm, we first modeled an anisotropic two-layered earth under the ocean, with a water depth of 1000 m and a water resistivity of 0.25 Ω·m. The first layer under the ocean is transversely isotropic with ρ_l = 1 Ω·m and ρ_t = 4 Ω·m and is 1000 m thick. The underlying half-space is isotropic with a resistivity of 2 Ω·m. We used our algorithm to calculate the electric field for the TI model, while concurrently we used the program from Jia et al. (2013) to calculate the electric field of 90 thin isotropic layers with alternative resistivities of 0.536 and 7.464 Ω·m and a thickness of 11.111 m. Based on work by Yin and Hodges (2003), we can calculate the equivalent resistivity ρ_l in the horizontal direction and ρ_t in the vertical direction as follows:

$$\rho_l = \frac{\sum_{i=1}^{N} h_i}{\sum_{i=1}^{N} h_i/\rho_i}, \quad \rho_t = \frac{\sum_{i=1}^{N} \rho_i h_i}{\sum_{i=1}^{N} h_i}. \tag{20}$$

The isotropic model and the equivalent TI model are given in Figure 1a. The transmitter is 50 m above the seabed, receiver is 30 m above the seabed, $AB = MN$ = 100 m, and the transmitting current is 500 A. As shown in Figure 1b, the results agree well. This confirms that the algorithm proposed in this paper has high precision.

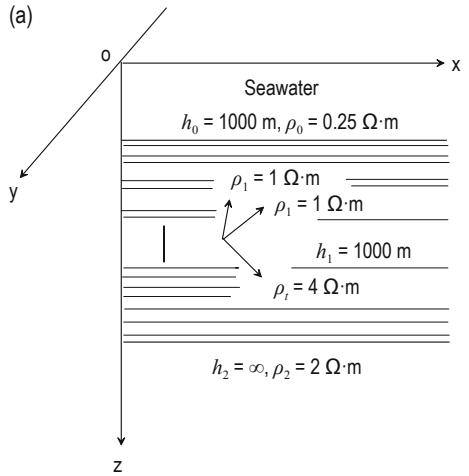

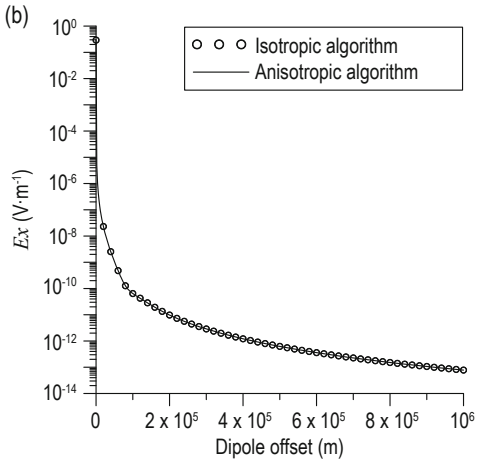

Fig. 1 (a) Anisotropic model for the accuracy check; (b) comparison of results from this paper and those from Jia (2013).

Identification of earth anisotropy from marine DC resistivity

As shown in Figure 2a, we assume the seawater depth to be 100 m and the resistivity of the seawater to be 0.25 Ω·m. The anisotropic formation is rotated around the *y*-axis, at the rotation angle ψ. Figure 2b shows polar plots of the apparent resistivity for different ψ values at a dipole offset of r_0 = 5000 m. The length of the radial vector to the origin at each point in the figure is the apparent resistivity value, while the direction of the radial vector corresponds to each survey array direction. Figure 2c shows the variation of the apparent resistivity versus dipole offset for different rotation angles ψ. The array is aligned in the *x*-direction.

From Figure 2b we can see that the apparent resistivity for the small dipole offset reflects the seawater resistivity. As the dipole offset increases, the anisotropy of the sea bottom takes effect and the apparent resistivity becomes $\rho_M / \sqrt{1+(\lambda^2-1)\sin^2\psi}$.

From the polar plots in Figure 2c we can see that: 1) since the dipole offset is large, the marine DC resistivity mainly reflects the influence from the anisotropic media under the seafloor. When the rotation angle is ψ = 0, the marine DC resistivity is similar to that on land (Shen et al., 2009). The apparent resistivity measured in different directions is equal to the average of the anisotropic resistivity ($\rho_M = \sqrt{\rho_l \times \rho_t}$); 2) when the rotation angle changes, the apparent resistivity along the *y*-axis rotation is greater than that in the perpendicular direction. This demonstrates an anisotropy paradox, i.e., the apparent resistivity axes are perpendicular to the true resistivity axes; 3) for this model, when the dipole array is aligned in the *y*-axis direction, the apparent resistivity is equal to the average resistivity $\rho_M = \sqrt{\rho_l \times \rho_t}$, and when the dipole array is aligned along the x-direction, the apparent resistivity is $\rho_M / \sqrt{1+(\lambda^2-1)\sin^2\psi}$ (Li, 2005), where $\lambda = \sqrt{\rho_t / \rho_l}$ is an anisotropic coefficient and ψ is the rotation angle around the y-axis; 4) from these observations, we can effectively identify earth anisotropy and determine the principal axis orientation of anisotropic formations from polar plots of the apparent resistivity.

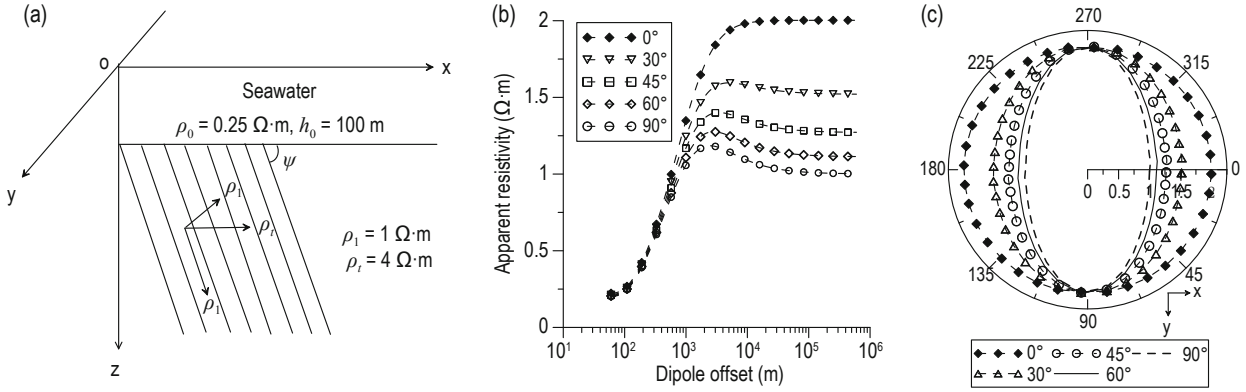

Fig.2(a) Dipping anisotropic earth under the ocean; (b) apparent resistivity vs. dipole offsets; (c) polar plot of apparent resistivity.

In order to review the distribution characteristics of the DC electric fields in both seawater and in the earth under the seafloor, we calculated the electric fields for the model in Figure 2a and the distributions of the electric field and current are displayed in Figure 3. The anisotropic strata are rotated at 0, 45, and 90 degrees around the *y*-axis. For comparison, we also show the electric field and current for an isotropic half-space with a resistivity of 1 Ω·m under the ocean. The black lines in the figure identify the horizontal electric dipole, and the electric field is normalized by the dipole moment.

From Figure 3, we see that: 1) the distributions of the electric current and electric field in an isotropic formation show symmetric field characteristic for a horizontal electric dipole. At the interface between the sea and the earth, the current and electric field changed. However, the tangential component of the electric field and the normal component of the current density are continuous; 2) when the rotation angle is 0 degrees, the horizontal current dominates; 3) when the principal resistivity is rotated 45 degrees, both the current flow and the contours of the electric field lean toward the current channeling direction; and 4) when the anisotropic formation is rotated 90 degrees, both the electric field and the current are squeezed to the vertical direction.

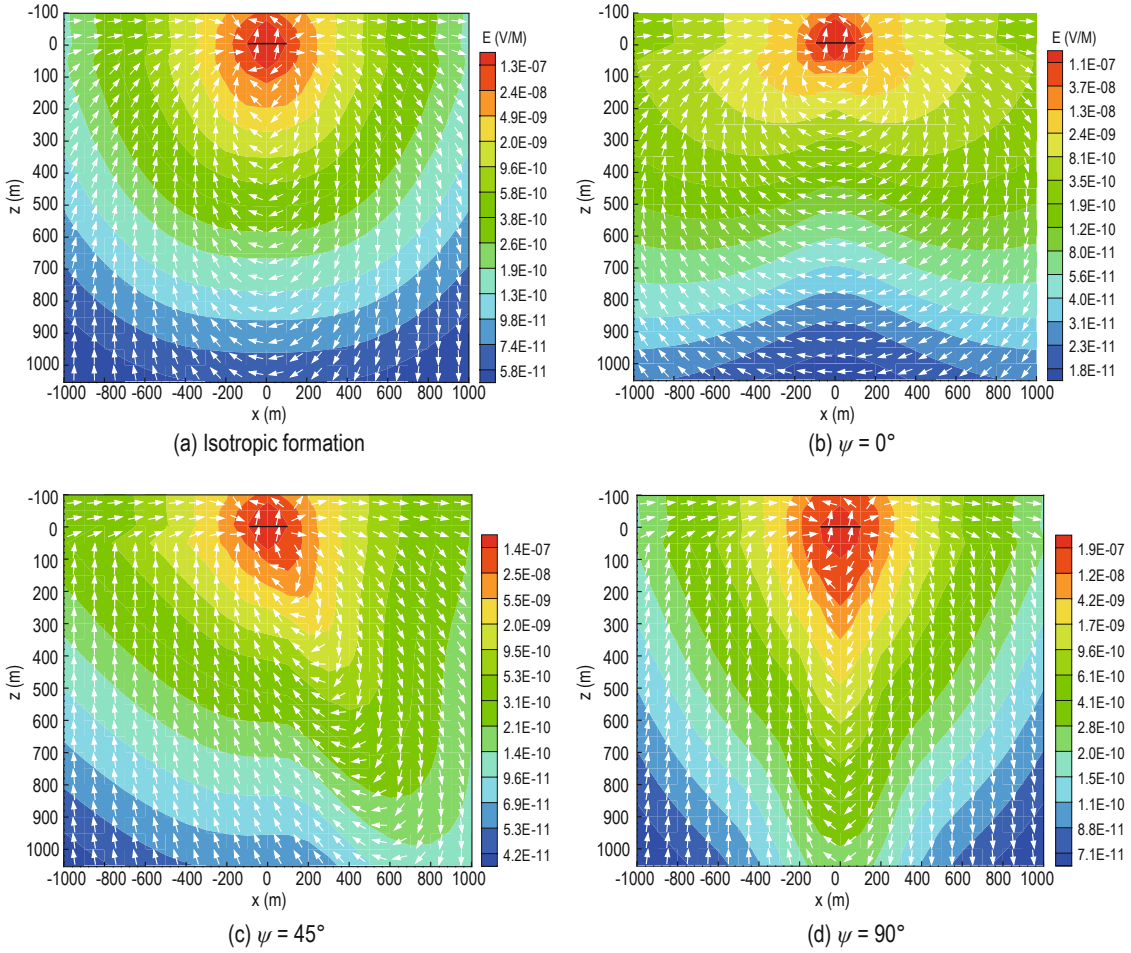

Fig.3 Distribution of the electrical field and current in an isotropic and anisotropic half-space under the ocean. The contours denote the electrical field, while the arrows show the current flow; the black lines denote the transmitting electrical dipole.

Identification of oil reservoirs under anisotropic formations

To investigate the DC resistivity method for offshore oil and gas exploration, we design an anisotropic background model with an embedded resistive reservoir. As shown in Fig. 4a, the resistivity of the seawater is 0.25 Ω·m. The resistivity of the anisotropic half-space along and perpendicular to the stratification are 1 Ω·m and 4 Ω·m, respectively. The resistive reservoir is 100 m thick with a resistivity of 100 Ω·m and a buried depth of 1000 m. The dipole parameters and transmitting current are the same as in Figure 1. To explore the effect of the anisotropic background on the oil and gas responses, we investigated the performance of the ratio of the apparent resistivity of an anisotropic half-space with an embedded reservoir to an anisotropic half-space. Figures 4b, 4c, and 4d show the results for rotation angles of 0, 45, and 90 degrees, respectively.

From the figures, we can see that: 1) in the shallow water area, the DC resistivity method can effectively identify the resistive reservoir. As the seawater depth

increases, the influence of the resistive thin layer on the apparent resistivity becomes weaker; and 2) due to the current channeling effect, the anomaly increases with an increasing rotation angle. This is because the current channeling results in more stimulation to the resistive reservoir.

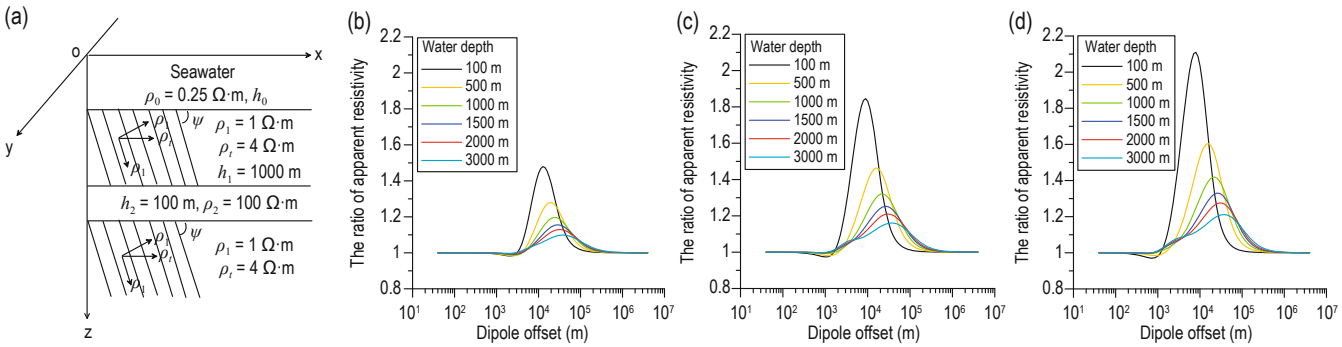

Fig.4 (a) Resistive reservoir in an anisotropic half-space under the ocean; (b)−(d) show the apparent resistivity ratios for different rotation angles and at different water depths.

(a) Resistive reservoir in an anisotropic half-space; (b) apparent resistivity ratio for ψ = 0°; (c) Apparent resistivity ratio for ψ = 45°; (d) Apparent resistivity ratio for ψ = 90°.

In order to study the anomalous characteristics of oil and gas reservoirs under the seafloor, we assumed that the seafloor resistivity remains constant (c.f. Figure 4a, where ρ_l = 1 Ω·m and ρ_t = 4 Ω·m, ψ = 90°) and calculated the ratio of the apparent resistivity (as defined in Figure 4) for different water depths. The results are shown in Figures 5a and 5b.

From Figure 5, we can see that: 1) as the water depth becomes shallower or the depth of the resistive reservoir decreases, the apparent resistivity ratio increases. This means that the DC resistivity method is effective for shallow-water oil and gas exploration; 2) as the seawater depth increases, the apparent resistivity ratio becomes weaker. In the present model, when the water depth is 1000 m and the target buried depth is 3000 m, the apparent resistivity anomaly is greater than 30%. However, from Figure 5b, we can see that to measure the anomaly of the resistive reservoir, there must be a very large offset (>20 km). This is difficult to achieve in practice and implies that the DC resistivity method is mostly suitable for shallow-water oil and gas exploration.

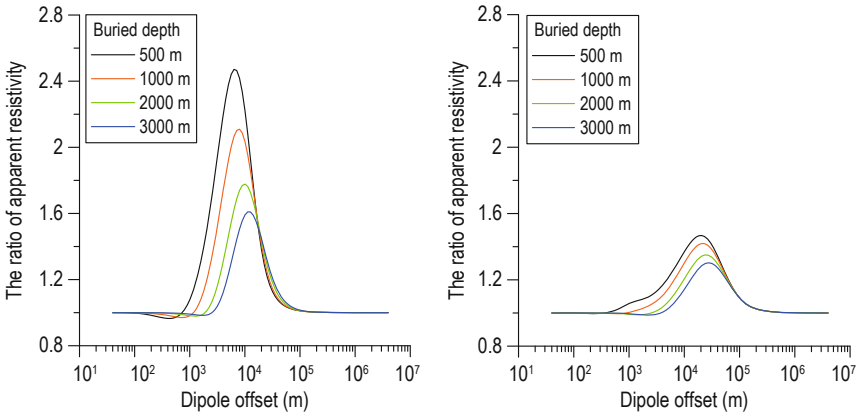

(a) Water depth 100 m (b) Water depth 1000 m

Fig.5 Apparent resistivity ratios for different water depths for different buried depths of the resistive reservoir.

Conclusions

We successfully applied the field continuation method to model the marine DC resistivity method for an anisotropic earth model. A comparison of our results with those from other algorithms demonstrates that the proposed algorithm has high modeling accuracy. From

our numerical experiment results, we draw the following conclusions:

(1) Earth anisotropy under the ocean can be identified from polar plots of the apparent resistivity. However, attention must be paid to the anisotropic paradox.

(2) Earth anisotropy significantly influences marine DC resistivity. Considering the sedimentary environment of the ocean, an anisotropic model is strongly recommended when interpreting marine DC resistivity data.

(3) The current channeling resulting from the anisotropy of the earth can increase the stimulation to the reservoir and increase the anomaly.

(4) The anomaly of the resistive reservoir is affected by both the water depth and the buried depth of the target layer. The shallower the water depth and the target burial depth, the greater is the anomaly.

(5) The marine DC resistivity method is especially suitable for oil and gas exploration in shallow-water areas.

Acknowledgements

We would like to thank Dr. Wang S. M. for his suggestions on improving the manuscript.

References

Allen, D., and Merrick, N., 2007, Robust 1D inversion of large towed geo-electric array datasets used for hydrogeological studies: Exploration Geophysics, **38**(1), 50−59.

Bronstein, I. N., and Semendjajew, K. A., 1979, Taschenbuch der Mathematik: B.G. Teubner Verlags Gesellschaft, Leipzig.

Cai, H. Z., Xiong, B., Han, M., and Zhdanov, M., 2014, 3D controlled-source electromagnetic modeling in anisotropic medium using edge-based finite element method: Computers & Geosciences, **73**, 164−176.

Fedynskiy, B. B., 1960, The Soviet Union's marine geophysical exploration: Geophysical Exploration, 1960 (2), 10−15.

Goto, T. N., Kasaya, T., Macgiyama, H., et al., 2008, A marine deep-towed DC resistivity survey in a methane hydrate area, Japan Sea: Exploration Geophysics, **39**, 52 −59.

Goto, T. N., Takekawa, J., Mikada, H., et al., 2013, Resistivity survey of seafloor massive sulfide areas in the Iheya north area, off Okinawa, Japan: Proceedings of the 11th SEGJ International Symposium, Yokohama, Japan, 298−301.

Inoue, M., 2005, Development and case studies of the new submarine electric sounding system: Geophysical Exploration, **58**, 241−250.

Jia, D. Y., Weng, A. H., Liu, Y. H., and Yin, C., 2013, Propagation of electromagnetic fields from a horizontal electrical dipole buried in ocean: Progress in Geophysics (in Chinese), **28**(1), 507−514.

Kong, F. N., Johnstad, S. E., Rosten, T., and Westerdahl1, H., 2008, A 2.5D finite-element-modeling difference method for marine CSEM modeling in stratified anisotropic media: Geophysics, **73**(1), F9−F19.

Kwon, H. S., Kim, J. H., Ahn, H. Y., and Yoon, J. S., 2005, Delineation of a fault zone beneath a river bed by a DC resistivity survey using a floating streamer cable: Exploration Geophysics, **36**, 50−58.

Li, J. M., 2005, Electric fields and electrical prospecting: Geological Publishing House, Beijing, 79−83.

Lile, O. B., Backe, K. R., Elvebakk, H., et al., 1994, Resistivity measurements on the sea bottom to map fracture zones in the bedrock underneath sediments: Geophysical Prospecting, **42**, 813–824.

Li, X. B., and Pedersen, L. B., 1991, The electromagnetic response of an azimuthally anisotropic half-space: Geophysics, **56**(9), 1462−1473.

Matias, M. J. S., and Habberjam, G. M., 1986, The effect of structure and anisotropy on resistivity measurements: Geophysics, **51**(4), 964−971.

Newman, G. A., Commer, M., and Carazzone, J. J., 2010, Imaging CSEM date in the presence of electrical anisotropy: Geophysics, **75**(2), F51−F61.

Shen, J. S., Guo, N. C., and Su, B. Y., 2009, Response characteristics of resistivity of anisotropic laminar formation in direct current electric sounding: Journal of China University of Petroleum, **33**(3), 59−65.

Tarits, P., Hussher, A., D'Eu, J. F., Balem, K., Hautot, S., and Girault, R., 2012, Free gas mapping with a new marine DC resistivity technique: SEG Technical Program Expanded Abstracts, 1−5.

Um, E. S., Harris, J. M., and Alumbaugh, D. L., 2010, 3D time-domain simulation of electromagnetic diffusion phenomena: A finite-element electric-field approach: geophysics, **75**(4), F115 −F126.

Von Herzen, R. P., Kirklin, J., and Becker, K., 1996, Geo-electrical measurements at the TAG hydrothermal mound: Geophysical Research letters, **23**, 3451−3454.

Wang, W., Wu, X. P., and Spitzer K., 2011, 3D DC anisotropic resistivity modeling using unstructured finite element method: International Workshop on Gravity, Electrical & Magnetic Methods and Their Applications,

Beijing, China, October **10–13**, 46 − 46.
Weidelt, P., 1999, 3-D conductivity models: Implications of electrical anisotropy: In: Oristaglio, M. and Spies, B., Eds. Three dimensional electromagnetics. Soc. Exploration Geophysics, 14−21.
Weng, A. H., and Zhu, S. A., 2010, Near sea-bottom DC sounding response for gas hydrate: Oil Geophysical Prospecting (in Chinese), **45**(3), 458−461.
Xu, T., and Dunbar, J. A., 2015, Binning Method for Mapping Irregularly Distributed Continuous Resistivity Profiling Data onto a Regular Grid for 3-D Inversion: Journal of Environmental and Engineering Geophysics, **20**(1), 1−17.
Yin, C. C., 2000, Geoelectrical inversion for a one-dimensional anisotropic model and inherent non-uniqueness: Geophysical Journal International, **140**, 11−23.
Yin, C. C., 2006, MMT forward modeling for a layered earth with arbitrary anisotropy: Geophysics, **71**(3), G115 −G128.
Yin, C. C., Ben, F., Liu, Y. H., and Cai, J., 2014, MCSEM 3D modeling for arbitrarily anisotropic media: Chinese J. Geophys. (in Chinese), **57**(12), 4110−4122.
Yin, C. C., and Hodges, G., 2003, Identification of Electrical Anisotropy from Helicopter EM Data: Symposium on the Application of Geophysics to Engineering and Environmental Problems, Environmental and Engineering Geophysical Society (EEGS), 419−431.
Yin, C. C., and Maurer, H. M., 2001, Electromagnetic induction in a layered earth with arbitrary anisotropy: Geophysics, **66**(5), 1405−1416.
Yin, C. C., and Weidelt, P., 1999, Geoelectrical fields in a layered earth with arbitrary anisotropy: Geophysics, **64**, 426−434.
Zhou, J. M., Li, X., Qi, Z. P., Sun, N. Q., and Wang, H. N., 2015, Simulation of 3D marine CSEM response in anisotropic media by coupled potential finite volume method: Near-Surface Asia Pacific Conference, Waikoloa, Hawaii, **7−10**, 343−346.

Yin Chang-Chun earned his Ph.D. in 1999 from the Department of Physics, TU University of Braunschweig, Germany. Before returning to China, he was a senior research scientist at FUGRO, Canada. In 2011, he joined the faculty of Jilin University, China. His research interests include electromagnetic forward modeling and inversion theory for airborne and marine electromagnetics.

Zhang Ping graduated from Jilin University in exploration technology and engineering (2014). He is currently a postgraduate in Jilin University and is mainly engaged in the modeling and inversion of electromagnetic anisotropic media.